Low-temperature spectroscopic studies of single molecules in 3-D and on 2-D hosts

Smit, R.

6

A DOUBLE-RESONANCE EXPERIMENT ON PERYLENE

In this chapter, I will lay out a theoretical and experimental framework for the detection of a resonance of a very weak singlet-to-triplet transition, where the region to look for this resonance is deduced from the phosphorescence spectrum in Chapter 3. Compared to other host/guest systems, the case of perdeuterated perylene in dibenzothiophene is complicated by an additional parameter, namely reverse intersystem crossing (rISC). I will show that rISC can be both helpful and problematic in this experiment and I will show how future experiments could be designed.

6.1. INTRODUCTION

6.1.1. EXPERIMENTS ON TRIPLET STATES

Since the detection of phosphorescence from triplet states is experimentally difficult, no experiments have been done on the excitation of triplet states from the ground state on single molecules. However, the stochastic intersystem crossing to the triplet state, the difference in the lifetimes of the three sublevels, the zero-field splitting between the states and highly-allowed transitions between triplet sublevels are such that it is possible to detect transitions *between* triplet sublevels. These transitions are generally captured by changes in the fluorescence signal as a function of a microwave excitation source, performed in a scheme called optically-detected magnetic resonance (ODMR). The first experiments on a single-molecule level, in 1993,[1,2] were already shortly conducted after the fluorescence signal from single molecules was detected for the first time in 1990.[3] In both works, the experiments were performed on single pentacene molecules in a *p*-terphenyl host matrix. A few years later, the first hyperfine-coupled nuclear spin of a carbon-13 atom was detected in the ODMR signal for the same pentacene.[4] Nowadays, ODMR is a common technique for reading out spin transitions in other systems, which typically allow for room-temperature operation, such as NV centers in diamond[5] and more recently, spin centers discovered in hexagonal boron nitride.[6] The latter two systems are different from single molecules in the sense that their ground state is already a triplet. Hence, no intersystem crossing or weak resonance to a spin state have to be involved. Systems such as NV centers have shown efficient coupling and control over many nuclear spins, where in extreme cases up to 50 nuclear spins could be mapped around an NV center.[7] Unlike singlet states, triplet states can be employed as nanosensors of magnetic field.[8]

Recently, there has been some renewed interest in the manipulation of spins in single molecules, due to the versatility and diversity of molecular systems. Recent work consists for instance on spin manipulation in ensembles of rare-earth Eu^{3+} molecular complexes,[9] organic radical molecules[10] and, interestingly, also by atomic force microscopy on the good old pentacene.[11] One of the key benefits of using a neutral aromatic molecule with a singlet ground state for spin manipulation, in special that of hyperfine-coupled nuclear spins, is that the electron spin can be turned off by de-excitation. In that case, the electron spin will not be a source of decoherence anymore for the nuclear spin, which could potentially increase the nuclear spin's coherence time, of particular uses for quantum memories. Moreover, molecular crystals are easily prepared and transferred. Furthermore, molecular crystals can be well implemented into photonic structures[12] and microcavities,[13,14] while dielectric antennas can boost collection efficiencies of photons close to unity.[15] All these properties make molecular systems attractive candidates for spin-photon interfaces.

Before such a spin-photon interface with single molecules can be realized, the coherent optical control of spin states has to be experimentally proven. In chapter 3, we recorded the phosphorescence spectrum of perdeuterated perylene in order to pin-point the spectral region where the weak resonance for the singlet-to-triplet transition would be located. In this chapter, I will report on the experiments that we set up to find this

resonance and the experimental challenges that come with it, such as the influence of reverse intersystem crossing.

6.1.2. THEORETICAL DESCRIPTION OF A THREE-LEVEL SYSTEM

The fluorescence and phosphorescence studies of perdeuterated perylene (to be called perylene-d12 from now on) in dibenzothiophene, in respectively Chapter 2 and Chapter 3, have made it possible to select a spectral region for a double optical resonance experiment on a single perylene-d12 molecule. The scheme for this experiment, shown in Figure 6.1, is similar to optically-detected magnetic resonance experiments, but with the major difference that the approach is entirely optical and initiated from the ground state. An alternative to initiation from the ground state is, in analogy to atomic physics, the so-called Λ-scheme, where the singlet-to-triplet transition is initiated from the singlet excited state, thus $S_1 \rightarrow T_1$. Given the energy of the singlet excited state and the energy of the triplet state, deduced respectively from the fluorescence and phosphorescence spectra, the $S_1 - T_1$ energy gap would be approximately 9,261 cm^{-1} (vacuum) or 1,080 nm (air). The considerably shorter wavelength for the $S_0 - T_1$ energy gap, namely around 784 nm, is experimentally easier to work with in combination with blue light for the $S_0 \rightarrow S_1$ transition. Hence, we will work with the scheme that is initiated from the ground state, called the V-scheme. In the V-scheme, a probe laser produces coherent cycles between the ground singlet and excited singlet state, which results in a measurable fluorescence signal. A pump laser scans the near-infrared (NIR) region for the spin-forbidden transition from the ground singlet state to the triplet state. This NIR region was determined in chapter 3 by the measured phosphorescence spectrum of perylene in the dibenzothiophene host in a region of interest determined by the inhomogeneous broadening around the 0-0 zero-phonon line. As a function of the NIR laser's frequency, the fluorescence signal may decrease or increase in intensity, depending on the steady-state population of the triplet states. In addition, we cannot ignore contributions of reverse intersystem crossing (rISC), which incoherently reduces the population of the triplet when the probe laser strongly excites the molecule's singlet transition. Furthermore, we assume that the NIR beam itself does not influence the rISC rate. To obtain an idea of the influence of reverse intersystem crossing by the probe beam we have to consider the rate equations, including coherences, for this double-resonance experiment.

In principle, there are three triplet sublevels with each of them having different intersystem crossing rates and lifetimes, but for the sake of simplicity I will group them into a single level. The three-level system of coupled rate equations has the following matrix form:

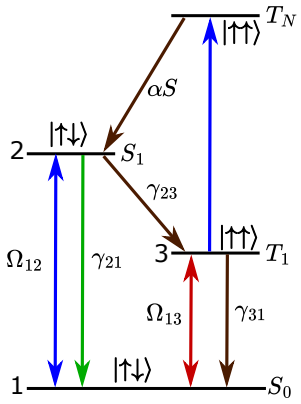

Figure 6.1.: Simplified Jablonski diagram of the three-level system, driven at resonance with the pump and probe laser. These resonances are indicated by a double arrow to account for stimulated emission. The relevant rates between the different levels are indicated next to the arrow. In addition, absorption from the probe laser to a higher triplet state is shown as the pathway for reverse intersystem crossing with total rate α proportional to the saturation parameter $S = I/I_s$ of the probe laser. The diagram is simplified in the sense that the three triplet sublevels are merged together.

$$\frac{d}{dt}\begin{bmatrix} p_{11} \\ p_{22} \\ p_{33} \\ p_{13} \\ p_{31} \\ p_{12} \\ p_{21} \end{bmatrix} = \begin{bmatrix} 0 & +\gamma_{21} & +\gamma_{31} & -\frac{1}{2}i\Omega_{13} & +\frac{1}{2}i\Omega_{13} & -\frac{1}{2}i\Omega_{12} & +\frac{1}{2}i\Omega_{12} \\ 0 & -\gamma_{21}-\gamma_{23} & +\alpha I & 0 & 0 & +\frac{1}{2}i\Omega_{12} & -\frac{1}{2}i\Omega_{12} \\ 0 & +\gamma_{23} & -\gamma_{31}-\alpha I & +\frac{1}{2}i\Omega_{13} & -\frac{1}{2}i\Omega_{13} & 0 & 0 \\ -\frac{1}{2}i\Omega_{13} & 0 & +\frac{1}{2}i\Omega_{13} & -\pi\Gamma_{13} & 0 & 0 & 0 \\ +\frac{1}{2}i\Omega_{13} & 0 & -\frac{1}{2}i\Omega_{13} & 0 & -\pi\Gamma_{13} & 0 & 0 \\ -\frac{1}{2}i\Omega_{12} & +\frac{1}{2}i\Omega_{12} & 0 & 0 & 0 & -\pi\Gamma_{12} & 0 \\ +\frac{1}{2}i\Omega_{12} & -\frac{1}{2}i\Omega_{12} & 0 & 0 & 0 & 0 & -\pi\Gamma_{12} \end{bmatrix} \begin{bmatrix} p_{11} \\ p_{22} \\ p_{33} \\ p_{13} \\ p_{31} \\ p_{12} \\ p_{21} \end{bmatrix} \tag{6.1}$$

The vectors contain the density matrix elements for the populations ρ_{11}, ρ_{22} and ρ_{33} of respectively the ground singlet, excited singlet and triplet states and the coherences captured in ρ_{13}, ρ_{31}, ρ_{12} and ρ_{21}. The parameters Ω_{12} and Ω_{13} are the Rabi frequencies of the $S_0 \rightarrow S_1$ and $S_0 \rightarrow T_1$ transitions. Furthermore, Γ_{12} and Γ_{13} are the homogeneous linewidths of both transitions, and are related to the decoherence times by $1/T_{2,12} = \pi\Gamma_{12}$ and $1/T_{2,13} = \pi\Gamma_{13}$. The rate γ_{21} is the decay rate of the excited singlet state, γ_{23} the intersystem crossing rate, γ_{31} the decay rate of the triplet and lastly, αI is the incremental decay rate of the triplet state due to reverse intersystem crossing, which is a function of the saturation parameter S of the probe laser. All detuning terms are ignored, as we plan to work at resonance. In Table 6.1, relevant parameters for equation 6.1 are listed. Most parameters have been acquired in our own experiments, but the linewidth of the $S_0 \rightarrow T_1$ transition has to be assumed. Although linewidths have been measured for ODMR transitions between triplet sublevels, nothing is known about the linewidth of an $S_0 \rightarrow T_1$ transition. Hence, we have to make the

assumption that the linewidth for the $S_0 \rightarrow T_1$ transition is similar to what is measured for transitions between triplet sublevels by ODMR. This, however, might not be true as ODMR transitions do not involve a change in molecular orbital. This, in principle, makes the $S_0 \rightarrow T_1$ transition sensitive to spectral diffusion that perturbs the $S_0 - T_1$ energy gap, on probably a similar timescale as for the $S_0 \rightarrow S_1$ transition. Assuming this spectral diffusion is negligible, the linewidth of the $S_0 \rightarrow T_1$ transition is given by the decoherence time $T_{2,13}$. In ODMR, the measured linewidth for hydrogenated molecules is typically in the order of a few MHz, while for deuterated molecules, the linewidth can narrow down to 100 kHz.[4] This is, however, not the homogeneous linewidth, because the measured linewidth is affected by slow spin dynamics (spectral diffusion) that broadens the linewidth during the relatively long acquisition times of an ODMR spectrum (in the order of seconds[16]). However, the homogeneous linewidth can be deduced from measurements on the decoherence time. Recently, the decoherence time was measured by atomic force microscopy (AFM) and was found for hydrogenated pentacene to be around 2.2 $\pm$ 0.3 µs, extending up to 16 $\pm$ 4 µs for deuterated pentacene.[11] Earlier pulse-sequence[17] and Hahn-echo[18] measurements confirm the $T_{2,13}$ found for hydrogenated pentacene with AFM. The measurements of the decoherence time indicate that the homogeneous linewidth of transitions between triplet sublevels is in the order of 150 kHz for hydrogenated pentacene and 20 kHz for deuterated pentacene, whereas the observed linewidths, respectively a few MHz and a few 100 kHz, are significantly broadened by spectral diffusion.

γ_{21} (s^{-1})	γ_{23}^{xy} (s^{-1})	γ_{23}^{z} (s^{-1})	γ_{31}^{xy} (s^{-1})	γ_{31}^{z} (s^{-1})	α $(s^{-1})/S$	Γ_{12} MHz	Γ_{13} kHz
2.2×10^8	532	46	118	16	18	~ 58	~ 20

Table 6.1.: Parameters included in the system of rate equations. All but the last parameter have been measured in experiment. The expected homogeneous linewidth of the transition to the triplet state is estimated from a decoherence time measurement of deuterated pentacene for transitions between triplet sublevels.[11] The dominant ISC rates and decay rates of the xy-triplet substates are used as values for γ_{23} and γ_{31} in equation 1.

The system of rate equations (equation 6.1) can be solved using the Laplace transform and this was done in MATLAB. The solutions for the populations are so lengthy that I will not display them here, but rather go directly to the results using the parameters displayed in Table 6.1. The solution has two variables of interest, namely the Rabi frequencies, Ω_{12}, for the $S_0 \rightarrow S_1$ transition and, Ω_{13}, for the $S_0 \rightarrow T_1$ transition. In general, the Rabi frequency scales with the square root of the laser intensity, thus with the optical field's amplitude. The Rabi frequency as a function of the saturation parameter S, for the singlet transition, can be approximated by:

$$\Omega_{12}(S) = \sqrt{\gamma_{21}\pi\Gamma_{12}} \times \sqrt{S} \approx 201\ MHz \times \sqrt{S}. \tag{6.2}$$

The solutions in Figure 6.2 are expressed in terms of the saturation parameter S (ratio of I/I_s), which indicates the Rabi frequency Ω_{12} in units of 201 MHz (see equation

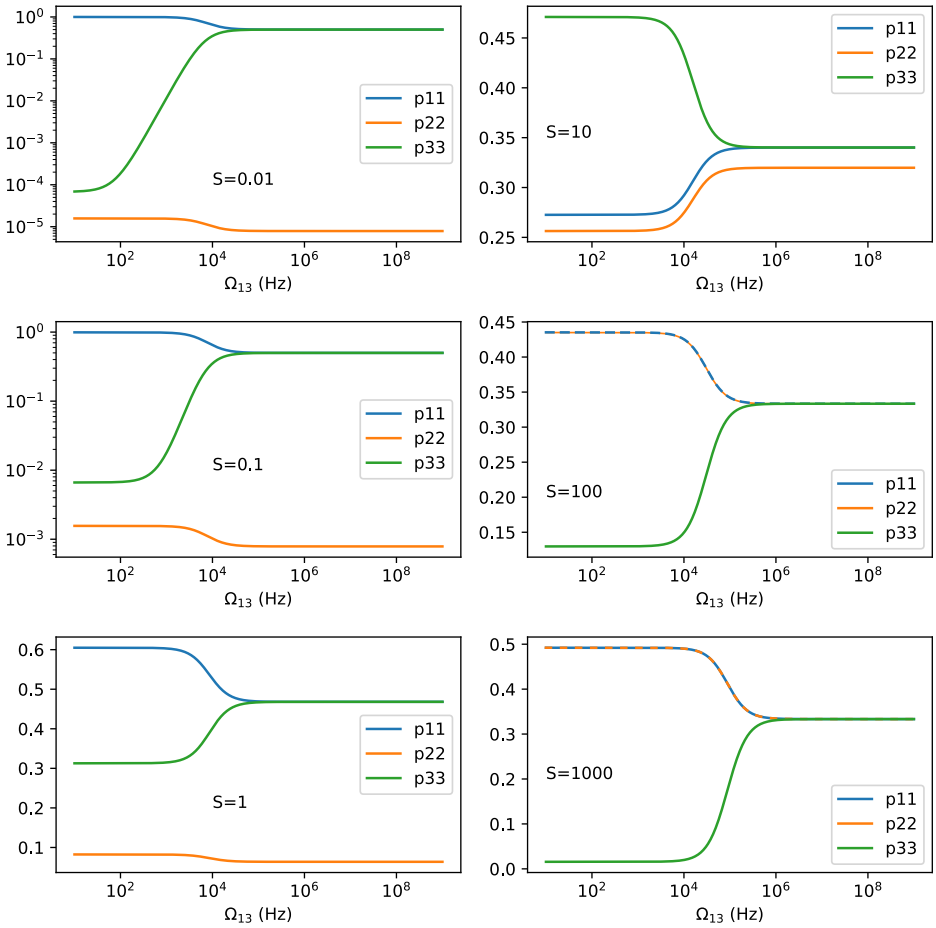

Figure 6.2.: Simulated fractions of populations of the three levels (their sum is always 1), where the triplet sublevels are grouped into a single level. The solutions have been processed for different levels of saturation for the singlet transition, given by the saturation parameter S, indicated in each figure panel. The Rabi frequency Ω_{12} as a function of the saturation parameter is determined by equation 6.2. At weak excitation, the population of the excited singlet is very low and therefore the populations are plotted on a log scale. At higher excitation intensities, starting from S=1, the populations are more comparable.

6.2). The saturation parameters, stretching from S=0.01 up to S=1000 are indicative of the experimentally attainable values, as measured in Figure 2.8 in Chapter 2. The

populations of the three levels are simulated as functions of how strongly we drive the $S_0 \rightarrow T_1$ transition and show where saturation of the triplet state occurs and in particular the effect it has on the excited state population ρ_{22} and thereby on the fluorescence signal. As a function of the saturation parameter S, there are three regimes that can be identified.

Regime 1. For the case of a weakly-excited molecule, thus $S \leq 0.1$ for Ω_{12}, the molecule spends most of the time in the ground state. In addition, intersystem crossing is not occurring frequently, as it grows linearly with the excited state population ρ_{22}. In that case, the coherent excitation of the triplet state would strongly increase the population, ρ_{33} of the triplet. Upon triplet excitation, the singlet excited state population is reduced and that leads to a decrease in the fluorescence signal. Of course, the model is simplified, and it is likely that the effect varies per triplet sublevel. Neglecting those variations per sublevel, the contrast of the $S_0 \rightarrow T_1$ transition's effect on the fluorescence can be up to 50% for S=0.01, decreasing slightly to 40% for S=0.1.

Regime 2. For the case of a moderately-excited molecule, thus $1 \leq S \leq 10$ for Ω_{12}, the higher saturation of the singlet excited state leads to strong intersystem crossing and a higher steady-state population for the triplet. At these excitation intensities, the effect of reverse intersystem crossing on the triplet state's population is still weak. Compared to regime 1, the effect of a coherent excitation of the triplet will now start to decrease the population in the triplet and in turn increases the fluorescence signal. The contrast in the fluorescence signal is relatively low, with only 10% for S=1 up to 20% for S=10.

Regime 3. For the case of a strongly-excited molecule, thus $S \geq 100$ for Ω_{12}, the effects of reverse intersystem crossing start to become noticeable. In steady state, the population of the triplet starts much lower due to shortened lifetimes. The coherent excitation of the triplet will, however, increase the population again and will therefore lower the fluorescence signal. The contrasts in the fluorescence signal are about 23% for S=100 and 32% for S=1000. For even higher excitation intensities, the populations of all three levels will equalize at a strong coherent excitation of the triplet. Hence, the theoretical maximum for the contrast is 33.3%. However, an important consequence of reverse intersystem crossing is that the Rabi frequency at saturation of the triplet rises as the lifetime of the triplet is shortened. In this regime, a higher saturation parameter S, will require more light intensity to induce enough transitions to the triplet state, which might be experimentally challenging.

The simplified model that I presented here will likely most resemble the case of strong excitation, where all three triplet sublevels have practically equal lifetimes due to reverse intersystem crossing (single exponential decay in the autocorrelation of fluorescence). All in all, given the three regimes in the simulation, the contrast of triplet absorption in the fluorescence will likely be optimal when working at low light intensity for the probe beam, which avoids both reverse intersystem crossing and strong intersystem crossing. However, the intermittent blinking of the fluorescence, with long duration times, will in

turn require relatively long averaging times of the fluorescence signal, as I will show in the next section.

6.1.3. EXPERIMENTAL CONDITIONS: CONTINUOUS WAVE EXCITATION

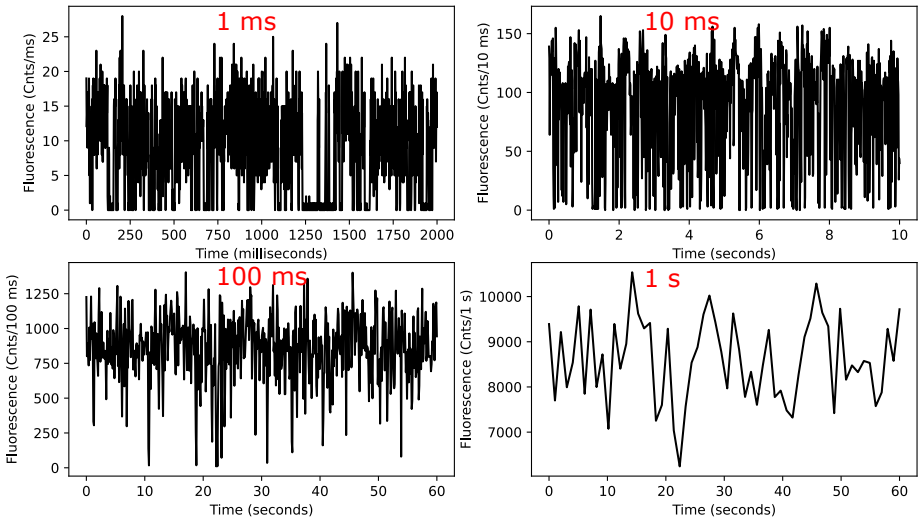

Figure 6.3.: Fluorescence signal from a single molecule, excited resonantly at S=0.1 and sampled to different time domains of 1 ms up to 1 s. Frequent blinking of the fluorescence due to intersystem crossing persists up to sampling rates of 10 Hz. Even at 1 sample per second the fluorescence signal fluctuates up to 20% around the mean. At 10 ms there are some periodic fluctuations present that might be due to external vibrations that couple to the cryostat.

There are two experimental routes for the double-resonance experiment. The simplest is to work in a continuous wave (CW) regime, where both lasers beams are always on. This is the basis for the simulations in Figure 6.2, which are solved for steady state. Another possibility is to perform the experiment in a pulsed scheme. This could potentially avoid reverse intersystem crossing, as long as the probe pulses are shorter than the rISC rate. However, the pulsed scheme has the disadvantage that the probe beam is only on for a short time and therefore the fluorescence signal is relatively low. The disadvantage of the CW regime is that the fluorescence signal tends to naturally fluctuate due to intersystem crossing and these fluctuations can last up to 100 ms. Hence, the fluorescence signal needs to be collected at low sampling rates. In Figure 6.3, some examples of sampling rates are shown. The figure shows that a 1 Hz sampling rate leads to a signal that fluctuates with a standard deviation of approximately 10%, with some single deviations of up to 20%. Even with this signal, a weak resonance with low contrast could be easily missed. Below S=1, the contrast of the fluorescence dip would

be at best 50% in the case of the simplified three level scheme, with a saturated Ω_{13}. Of course, beyond saturation of the $S_0 \rightarrow T_1$ transition, the linewidth will be power broadened. This power broadening scales with the square root of the laser intensity as:

$$\Gamma(I) = \Gamma_0 \sqrt{1 + I/I_s}. \tag{6.3}$$

At this point it is not clear whether we can obtain significant power-broadened linewidths with the experimentally attainable intensities of the NIR laser, which is in the tens of mW range or, in best case focused to a diffraction-limited spot, amounts to about 1-10 MW/cm^2. To make a guess of the saturation intensity of the triplet in order to find out how much we can power-broaden the linewidth, given the assumption that the linewidths are similar to those found in ODMR experiments, we can consider the following expression for the saturation intensity:

$$I_{s,13} \propto \frac{\gamma_{31}\Gamma_{13}}{|\mu_{13}|^2}, \tag{6.4}$$

where μ_{13} is not introduced before and describes the transition dipole moment for the $S_0 \rightarrow T_1$ transition. From experiment, we know the saturation intensity of the $S_0 \rightarrow S_1$ transition and therefore we can directly compare their values:

$$\frac{I_{s,13}}{I_{s,12}} = \frac{|\mu_{12}|^2\gamma_{31}\Gamma_{13}}{|\mu_{13}\gamma_{21}\Gamma_{12}|^2} \approx \frac{|\mu_{12}|^2}{|\mu_{13}|^2} \times \frac{25 \times 10^3\ Hz}{58 \times 10^6\ Hz} \times \frac{118\ s^{-1}}{2.2 \times 10^8\ s^{-1}}. \tag{6.5}$$

It helps that the assumed linewidth of the $S_0 \rightarrow T_1$ transition of approximately 25 kHz with respect to the 58 MHz of the $S_0 \rightarrow S_1$ transition reduces the ratio. Also, the low rate of γ_{31} as compared to γ_{21} works in our advantage and reduces the ratio. However, the transition to the triplet is forbidden and therefore has a weaker transition dipole moment. An experiment on $S_0 \rightarrow T_1$ absorption for pure perylene crystals found an estimated oscillator strength of 10^{-10},[19] which is proportional to the square of the transition dipole moment. The same group also estimated the oscillator strength of the $S_0 \rightarrow S_1$ transition of perylene to be around 0.44[20] and therefore we have 10 orders of magnitude difference. With these numbers we obtain a ratio of the saturation intensity for the T_{xy} triplet sublevels as compared to the saturation intensity of the singlet of about a factor 0.8, which makes them practically equal. For the T_z triplet sublevel the ratio would be 0.11. Physically this makes sense: although the transition is very weak, only a limited number of absorbed photons are necessary to saturate the level, because it is much longer lived than the singlet excited state. In addition, if the transition is very narrow this enhances absorption, as long as the laser linewidth is comparable or narrower. However, if there would be significant broadening of the homogeneous linewidth, to a value similar for the $S_0 \rightarrow S_1$ transition, the ratio would be around 2,400. With the power densities available of up to 1-10 MW/cm^2 as compared to the saturation intensity of the singlet of 22 W/cm^2 (see Chapter 2), we can supply 4-5 orders of magnitude higher intensities. This could broaden the transition by 100-300 times, leaving us in best case with a linewidth of 4.7-15 MHz for the T_{xy} triplet sublevels and 13-40 MHz for the T_z triplet substate. With a laser of 100 kHz linewidth (see section 6.2) and similar scan resolution per measurement point we could therefore pinpoint this transition out of the natural fluctuations present in the fluorescence signal. Of course, the

above argument, based on the assumption that the homogeneous linewidth is around 20 kHz, only works when rISC is negligible, because it increases the rate of γ_{31} and thus increases the amount of laser power that is necessary to obtain saturation of the triplet.

6.1.4. PULSED EXCITATION

To eliminate random fluctuations due to intersystem crossing (ISC) from the data, we could as an alternative method resort to pulsed excitation. In this case, the singlet transition is shortly excited and fluorescence is collected in the same time window. When photons are measured, the molecule is likely not in the triplet state. Hence, we can supply a pulse of NIR light to try to excite the triplet state. Subsequently, we can supply another pulse of blue light and measure if we are in the triplet state again, as then there would be no photons coming out if that would be the case. The duration of the blue pulse length should however be long enough to collect enough photons from fluorescence, while avoiding rISC, which is probably in the 1-100 µs regime. With these pulse durations and excitation beyond saturation, we can record 0.5-50 photons for each pulse on average.

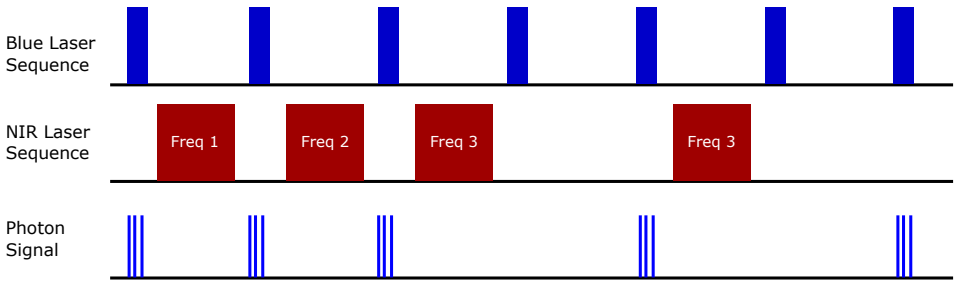

Figure 6.4.: Proposed sequence of pulses to detect a resonant transition to the triplet state. The blue laser pulse measures if the molecule is in the ground state by inducing fluorescence. With the NIR pulse we try to induce a transition to the triplet state. If the NIR pulse is at resonance with the triplet state, the subsequent blue pulse shouldn't generate any photon.

The duration of the NIR pulse is more difficult to determine, as it depends on the Rabi frequency that we obtain with the light intensity that we use. At saturation, the Rabi frequency of the triplet would be in the same manner as for the singlet, calculated to be around 2.7 kHz for the T_{xy} states and 1.0 kHz for the T_z state (equation 6.2). When we would have laser intensities of 1-10 MW/cm^2, the Rabi frequency would amount to 0.65-2 MHz for the T_{xy} states and also 0.65-2 MHz for the T_z state. Therefore, the frequency scale of the pulse can possibly be made shorter than the decoherence rate of around 62.5 kHz (=$\pi\Gamma_{13}$). For these very short pulses, the pulse length could fit integer multiples of a π-pulse + $2n\pi$ (additional Rabi cycles) and then the molecule would end up in the triplet state at the end of the pulse. However, if the pulse fits $2n\pi$ Rabi cycles,

the system would end up in the ground state. With effective π-pulses, we could obtain the best contrast in the signal. However, it is difficult to experimentally determine the Rabi frequency, without knowing anything yet about the coherent interaction of the NIR laser with the triplet state. Therefore it is best to employ a pulse duration that is significantly longer than the decoherence time (around 16 µs). In that case, we firstly prevent that we unintentionally choose a pulse length that effectively de-excites the molecule and secondly, we prevent the case where our Rabi frequency would be overestimated and thus too low to excite the molecule into the triplet at all. However, for long pulses the contrast would be only 50%, as the molecule will be half the time in the excited triplet and half the time in the ground state at the end of the pulse.

Building up a setup that involves the use of pulses can be convenient for later experiments, once the resonances of the triplet are found, that use pulse sequences to probe the coherence properties of the triplet. However, coherence properties of the triplet states can also be measured in continuous wave using time-correlated single-photon counting, i.e. an antibunching histogram. Overall, a continuous-wave experiment is easier to setup and will therefore be part of the next section.

6.2. EXPERIMENTAL DETAILS

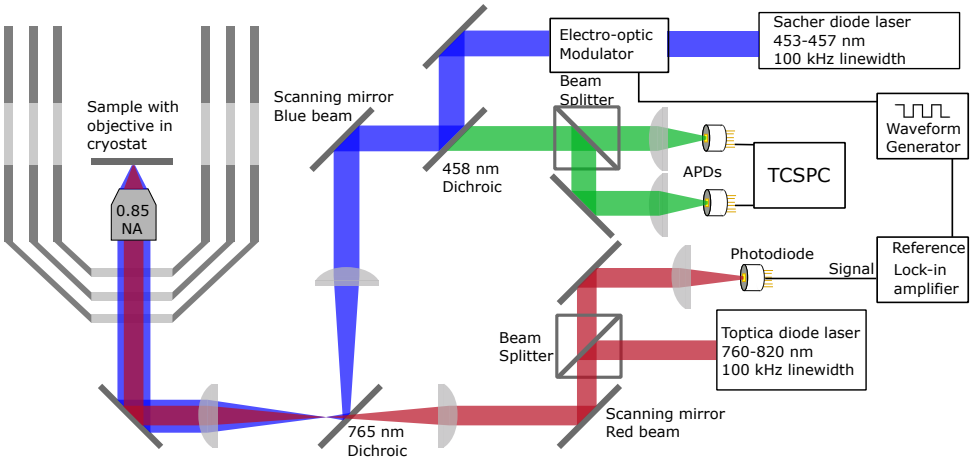

Figure 6.5.: Schematic of the experimental setup for the double-resonance experiment. The blue and red laser beam are combined at the 765 nm dichroic mirror and directed towards the objective in the cryostat. The avalanche photodiodes (APD's) collect fluorescence from the blue beam and the photodiode recovers the scattered light from a particle or gold film and transmits this signal to a lock-in amplifier. The blue beam can be modulated or pulsed using an electro-optic modulator. Both beams also have their own scanning mirrors for making small adjustments.

Whether we would resort to CW or pulsed excitations does not matter much for the basic experimental setup. In the experiment, the blue (Sacher diode laser 454-457 nm tunable range, 100 kHz linewidth) and near-infrared (NIR) laser (Toptica DL Pro HP, 760-820 nm tuning range, 100 kHz linewidth) beam will have to be focused onto the molecule to make sure that we can obtain the highest laser power densities possible. The required wavelengths for the two lasers, which are 454 nm and 784 nm, are quite far from each other and therefore we have to make sure that they are well overlapped in the focal plane and therefore are corrected for chromatic aberrations present in the optics. The overlapping of the two beams can be done through imaging of a small diffraction-limited particle, while trying to overlap the two images by moving one of the beams. Other methods include the use of pump-probe techniques. We considered using two-photon absorption, but the combination of photons from the two beams is in the ultraviolet (UV), which is not the right spectral region for our objective when we would have to collect UV fluorescence. Another possibility is the use of photothermal microscopy, but this principle has only been proved to work close to room temperature due to the required presence of a liquid. Fortunately, the effects of temperature on the alignment of our confocal setup are limited, as we always align at room temperature and directly use the setup for low temperature, without any further adjustments. Therefore we equipped the setup with components that make photothermal imaging possible. Figure 6.5 shows a schematic of the setup that we constructed. To maximize the excitation power and increase the amount of collected fluorescence we make use of dichroic mirrors, where a dichroic mirror at 458 nm (FF458-Di02-25x36, Semrock) passes the red-shifted fluorescence from perylene. The two laser beams are combined at a 765 nm long pass dichroic mirror (FF765-Di01-25x36x2.0, Semrock), which transmits the NIR light, but reflects the blue and fluorescence from perylene. Both laser beams have their own scanning mirror (Newport FSM-200) and therefore slight adjustments can be made for each beam separately. For the alignment procedure, we included an electro-optic modulator (Model 370 from Conoptics, controlled by a high-voltage amplifier DIV 20 from Qioptiq, which amplifies the signal from a waveform generator from Tektronix) in the beam path of the blue beam, which acts as the pump beam. With this EOM we can turn the beam on and off, to modulate heating of an object or surface, as part of the photothermal effect.[21] In turn, we can also use this EOM to generate pulses for the pulsed excitation scheme. The NIR beam is directed to a photodiode, which measures the scattered light intensity from a particle that is being transiently heated by the pump beam. The modulated heating on the particle creates a modulated diffusion of heat around the particle and in turn modulates the refractive index of the immersion oil (Olympus, Type-F, n=1.518) around the particle. Changes in the immersion fluid's refractive index modifies the amount of light scattered from the particle. The signal of the scattered light onto the photodiode is connected to a Lock-in amplifier (SR844 from Stanford Research Systems), which extracts the photothermal signal in a narrow bandwidth around the modulation frequency. The amplitude of the lock-in signal is then a measure of the photothermal effect. By walking the two laser beams, we can find the maximum of this effect and that will be at the point where the two beams are well overlapped.

As the power of the blue laser is limited, the photothermal signal was rather weak, which in addition was lower due to the weak collection efficiency of the air objective (0.85 NA). The weak signal made it difficult to measure a photothermal signal from single, rather big, 80 nm gold spheres. However, the photothermal signal could be obtained on clusters of these spheres and on a 300 nm thick gold film. To obtain a good signal to noise for the photothermal signal, we used a gold film on glass, covered with another glass slip. At the interface we put a layer of immersion oil as the medium.

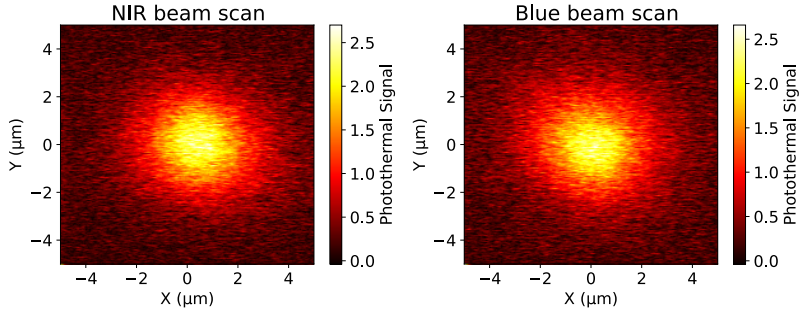

Figure 6.6.: Photothermal images of a gold film, measured at room temperature. The blue laser intensity is 80 µW at a 1 MHz modulation frequency and the NIR laser around 1 mW. The left image corresponds to a fixed blue beam (heating beam) and a scanned NIR beam (probe beam). On the right, the NIR beam is fixed and the blue beam is scanned. The images show a Gaussian point spread function with a width of about 2 µm.

6.3. RESULTS AND DISCUSSION

6.3.1. EXPERIMENTS WITH STRONG REVERSE INTERSYSTEM CROSSING

Due to the limited time for experiments left before the end of my PhD trajectory, we decided to start the experiment in a simple way by profiting from the enhanced stability of the fluorescence signal by reverse intersystem crossing. A positive effect of rISC is that the fluorescence signal is steady, even for much shorter integration times compared to the necessary integration time of up to 1 second in Figure 6.3, in the case of weak excitation of the singlet. Moreover, the broader linewidth limits the influence of weak spectral diffusion, while the laser's frequency remains fixed (Figure 6.7). This also makes it unnecessary to employ a feedback algorithm that keeps the laser in resonance with the molecule. However, the negative effect is that the saturation intensity of the transition to the triplet increases as the triplet lifetime is reduced. Assuming that we have enough laser intensity available, this is not necessarily a bottleneck.

To make sure that we only have a single emitter present with good single-photon statistics and coherence properties, we can record the antibunching histogram of the

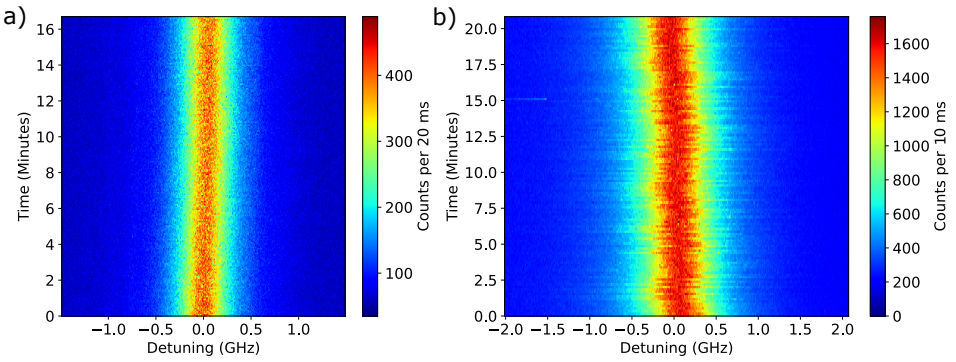

Figure 6.7.: Examples of time traces of excitation spectra, taken at high excitation intensities. The colors in the heatmap are relatively uniform due to shortened shelving in the triplet state. The molecule in panel (a) has a linewidth broadened to 496 MHz, at about 100 times saturation intensity. The molecule in panel (b) has a linewidth of 770 MHz, at about 225 times the saturation intensity. This molecule has a particularly uniform color in the excitation spectra, given that the integration time is only 10 ms and indicates very short dwell times in the triplet state. With the highest excitation intensity available, we could reduce triplet lifetimes down to 60 µs.

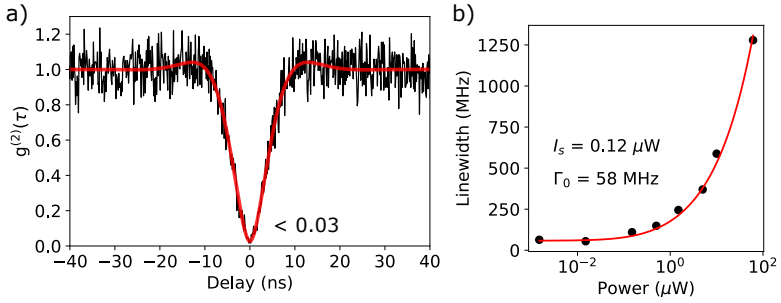

Figure 6.8.: Panel (a) shows an antibunching histogram at a low excitation intensity, showing a high single-photon purity with $g^{(2)}(0) < 0.03$. The fitted Rabi frequency Ω_{12} is around 200 MHz. Panel (b) shows linewidth broadening of a single perylene-d12 molecule at a range of excitation intensities. The fitted saturation intensity I_s, obtained by the of the experimental data to equation 6.3, amounts to 0.12 ± 0.01 µW.

fluorescence signal at resonance with the 0-0 ZPL. At low excitation intensities, we can limit the influence of background and obtain a high single-photon purity of more than 97%, as shown in Figure 6.8a. Furthermore, at high excitation intensities we can

observe clear Rabi oscillations in the photon statistics (Figure 6.9). This allows the extraction of the Rabi frequency, Ω_{12}, using equation A.8 in Appendix 1. The excitation intensities in the figure can be related to the saturation intensity extracted from the linewidth broadening curve in Figure 6.8b. The Rabi frequency at saturation is then estimated to be around 200 MHz for Figure 6.9c and 6.9d, which due to higher laser intensities have lower uncertainties in the measured laser power. This corresponds well to the calculated value in equation 6.2, which, based on intramolecular rates, states that the Rabi frequency at saturation is around 201 MHz. The homogeneous linewidth is 58 MHz, similar to the narrowest linewidths found for perylene-d12 in dibenzothiophene (see also Chapter 2).

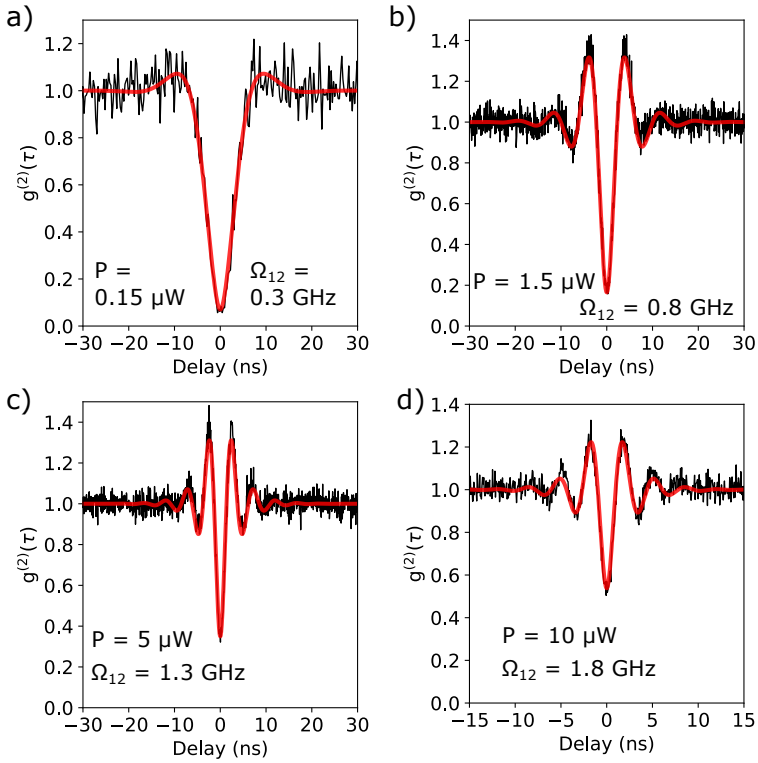

Figure 6.9.: Series of antibunching histograms of a single molecule, taken at increasing excitation intensities. Higher excitation intensities are possible, but the Rabi oscillations and dip will not be visible anymore due to uncertainty in the timing resolution caused by jitter of the detector (documented to be around 350 ps).

In experiments, it turned out to be a challenge to find a molecule that stays in resonance with the laser for more than a minute while the linewidth is (near) lifetime limited. However, a power-broadened linewidth in the order of 500 MHz was almost always enough to keep a steady resonance without additional feedback. The observed

spectral diffusion could be caused by the poor crystallization of the host through freeze-quenching, which could be improved by sublimation techniques or perhaps low-temperature annealing.

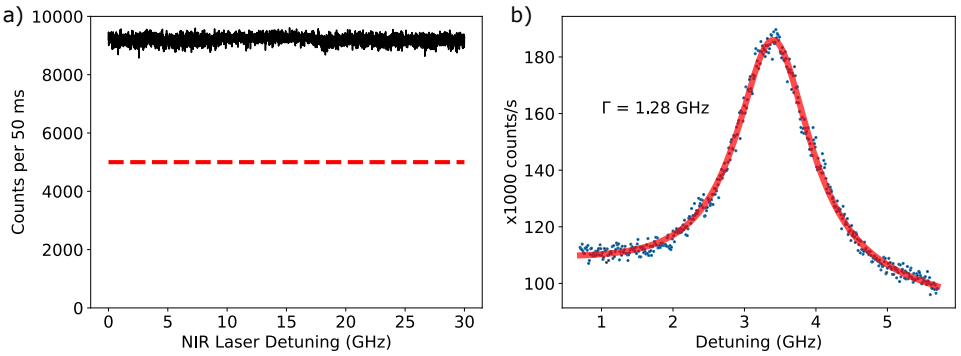

Figure 6.10.: a) Fluorescence signal of a single perylene-d12 molecule recorded at resonance with the 0-0 ZPL at a high excitation intensity (S ≈ 486), while the NIR laser is scanned over 30 GHz. The background signal (red dashed line) amounts to a relatively high 100 kcnt/s, while the fluorescence signal (black data) is around 80 kcnt/s. The fluorescence signal is very stable within the relatively short integration time of 50 ms due to strong reverse intersystem crossing. No resonance with the triplet was detected in this scan. Panel (b) shows the Lorentzian profile of the molecule in panel (a). The strong excitation power-broadens the linewidth to 1.28 GHz, which from the homogeneous linewidth of about 58 MHz amounts to a saturation parameter $S \approx 486$. Given that rISC typically scales with a rate of 18 s^{-1} as factors of S, triplet lifetimes have probably reduced to around 110 µs.

As shown in Figure 6.10, the integration time of the fluorescence, recorded at resonance, can be scaled down to 50 ms, or perhaps less, without significant drops in fluorescence present. This is very different from the situation displayed in Figure 6.3, which describes the case of a weak excitation of the 0-0 ZPL. Unfortunately, we were not able to detect a resonance within a larger scan of more than 2 nm around the center of the inhomogeneous broadening of the 0-0 ZPL found in the phosphorescence spectrum, shown in Figure 6.11. The measurement shows that it is possible to remain at resonance with the 0-0 ZPL of the singlet transition for up to 2 hours (total scan duration) without inducing spectral diffusion due to the high intensity light of about 2 MW/cm^2. At saturation of the triplet, a maximum contrast of 33 % is expected, yet no dip in the fluorescence signal is more significant than 10 %. There are some upward jumps present in the fluorescence signal, but they were not reproducible and might have originated from spectrally-diffusing molecules that intermittently jumped into resonance with the laser.

Compared to the usual saturation intensity of 22 W/cm^2 for the singlet, the intensity of 2 MW/cm^2 is a factor 10^5 higher. The linewidth could therefore, focusing on the T_{xy} triplet substates amount to 6.7 MHz, taking into account that the saturation intensity of the triplet is about a factor 0.8 compared to the singlet (equation 6.4). However, this value is based on the case without rISC and moreover, this only applies when both laser beams are at the same focal point and all the NIR laser power is focused onto the molecule. At the broadened linewidth, displayed in Figure 6.10b, the triplet lifetimes have reduced to around 110 µs. Hence, the saturation intensity will scale up as well. The ratio of the saturation intensity with rISC as compared to the case without rISC is calculated by:

$$R(S) = \frac{I_{s,with\ rISC}}{I_{s,without\ rISC}} = \frac{\gamma_{31} + \alpha S}{\gamma_{31}}. \tag{6.6}$$

With $S \approx 486$, the ratio is approximately 75. Taking into account this adjusted saturation intensity, the used laser power is only 1700 times higher than the theoretical saturation intensity and translates into a broadened linewidth of only 0.8 MHz, at best conditions. Hence, the step size of 6 MHz in the scan is too large. Still the experimental data shows that the experiment is conceptually feasible and that a molecule can be measured for prolonged times at resonance with the 0-0 ZPL, without significant drifts in the fluorescence signal. This indicates that the setup is mechanically stable enough. Moreover, no spectral diffusion was observed on the singlet resonance, despite the large intensity of the NIR laser beam.

6.4. CONCLUSION AND OUTLOOK

In this chapter, we have reported on the theoretical framework of the double-resonance experiment and first trial experiments. Although the presence of reverse intersystem crossing can be helpful by reducing the integration time needed for each data point, due to the enhanced stability of the fluorescence signal, it can also be a limiting factor in the experiments. The presence of rISC increases the required intensity to saturate the transition to the triplet and may suppress broadening of the linewidth at the laser intensities that we have available. This may in turn require smaller incremental steps in the laser frequency and increase the duration of the NIR region scan, around the center the center of the inhomogeneous broadening found in the phosphorescence spectrum.

The long duration of the scan in Figure 6.11, which due to strong rISC should perhaps be taken at smaller incremental steps, would in future require automatization. Therefore it would be better to perform this experiment in a closed-cycle cryostat, which can maintain a low temperature for a longer time without having to intervene manually. The use of solid immersion lenses could also help to increase the laser power densities on the molecule and increase the fluorescence signal. It can also be helpful to further reduce the background fluorescence in the signal to increase the contrast of transitions to the triplet, which could probably be achieved by lowering the concentration of perylene molecules inside the crystals.

Another possibility is the use of hydrogenated perylene (perylene-h12), instead of

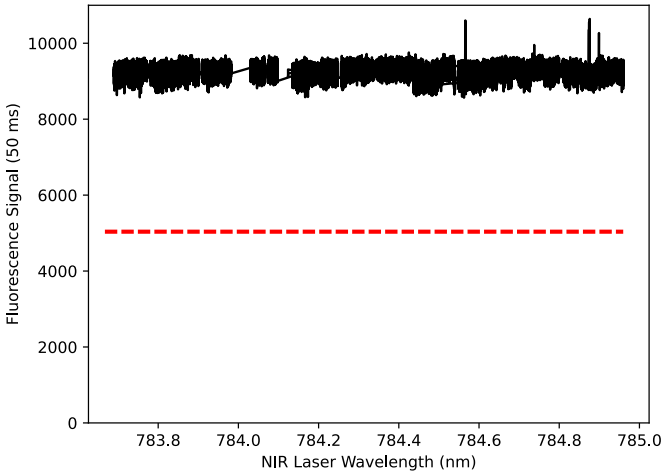

Figure 6.11.: Long range scan of the NIR laser with single-molecule fluorescence recorded at resonance with the 0-0 ZPL. The red dashed line represents the background level. There are sometimes gaps in the scan due to jumps in the laser. Peaks in the fluorescence were not reproducible and could be from spectrally-diffusing molecules. The scan was recorded with a 6 MHz resolution for the NIR laser, at a light intensity of 2 MW/cm^2 in a diffraction-limited spot of 1 µm. The whole scan was recorded over a period of 2 hours.

perdeuterated perylene (perylene-d12). For perylene-h12, the linewidth is expected to be around 8 times broader due to the shorter decoherence time. However, the spectral sites of perylene-h12 may be shifted relative to those of perylene-d12, which was for instance measured to be in the order of tens of cm^{-1} for pentacene-h14 and pentacene-d14 in *p*-terphenyl.[4] This may require a repetition of the phosphorescence experiment with perylene-h12.

REFERENCES

(1) Köhler, J.; Disselhorst, J. a. J. M.; Donckers, M. C. J. M.; Groenen, E. J. J.; Schmidt, J.; Moerner, W. E. *Nature* **1993**, *363*, 242–244.

(2) Wrachtrup, J.; von Borczyskowski, C.; Bernard, J.; Orrit, M.; Brown, R. *Nature* **1993**, *363*, 244–245.

(3) Orrit, M.; Bernard, J. *Physical Review Letters* **1990**, *65*, 2716–2719.

(4) Köhler, J.; Brouwer, A. C.; Groenen, E. J.; Schmidt, J. *Science (New York, N.Y.)* **1995**, *268*, 1457–1460.

(5) Gruber, A.; Dräbenstedt, A.; Tietz, C.; Fleury, L.; Wrachtrup, J.; Borczyskowski, C. v. *Science* **1997**, *276*, 2012–2014.

(6) Gottscholl, A.; Diez, M.; Soltamov, V.; Kasper, C.; Sperlich, A.; Kianinia, M.; Bradac, C.; Aharonovich, I.; Dyakonov, V. *Science Advances* **2021**, *7*, eabf3630.

(7) Van de Stolpe, G. L.; Kwiatkowski, D. P.; Bradley, C. E.; Randall, J.; Breitweiser, S. A.; Bassett, L. C.; Markham, M.; Twitchen, D. J.; Taminiau, T. H. Mapping a 50-spin-qubit network through correlated sensing, 2023.

(8) Taylor, J. M.; Cappellaro, P.; Childress, L.; Jiang, L.; Budker, D.; Hemmer, P. R.; Yacoby, A.; Walsworth, R.; Lukin, M. D. *Nature Physics* **2008**, *4*, 810–816.

(9) Serrano, D.; Kuppusamy, S. K.; Heinrich, B.; Fuhr, O.; Hunger, D.; Ruben, M.; Goldner, P. *Nature* **2022**, *603*, 241–246.

(10) Gorgon, S.; Lv, K.; Grüne, J.; Drummond, B. H.; Myers, W. K.; Londi, G.; Ricci, G.; Valverde, D.; Tonnelé, C.; Murto, P.; Romanov, A. S.; Casanova, D.; Dyakonov, V.; Sperlich, A.; Beljonne, D.; Olivier, Y.; Li, F.; Friend, R. H.; Evans, E. W. *Nature* **2023**, *620*, 538–544.

(11) Sellies, L.; Spachtholz, R.; Bleher, S.; Eckrich, J.; Scheuerer, P.; Repp, J. *Nature* **2023**, *624*, 64–68.

(12) Ren, P.; Wei, S.; Liu, W.; Lin, S.; Tian, Z.; Huang, T.; Tang, J.; Shi, Y.; Chen, X.-W. *Nature Communications* **2022**, *13*, 3982.

(13) Wang, D.; Kelkar, H.; Martin-Cano, D.; Utikal, T.; Götzinger, S.; Sandoghdar, V. *Physical Review X* **2017**, *7*, 021014.

(14) Pscherer, A.; Meierhofer, M.; Wang, D.; Kelkar, H.; Martín-Cano, D.; Utikal, T.; Götzinger, S.; Sandoghdar, V. *Physical Review Letters* **2021**, *127*, 133603.

(15) Chen, X.-W.; Götzinger, S.; Sandoghdar, V. *Optics Letters* **2011**, *36*, 3545–3547.

(16) Brown, R.; Wrachtrup, J.; Orrit, M.; Bernard, J.; von Borczyskowski, C. *The Journal of Chemical Physics* **1994**, *100*, 7182–7191.

(17) Wrachtrup, J.; Von Borczyskowski, C.; Bernard, J.; Orrit, M.; Brown, R. *Physical Review Letters* **1993**, *71*, 3565–3568.

(18) Wrachtrup, J.; von Borczyskowski, C.; Bernard, J.; Brown, R.; Orrit, M. *Chemical Physics Letters* **1995**, *245*, 262–267.

(19) Clarke, R. H.; Hochstrasser, R. M. *Journal of Molecular Spectroscopy* **1969**, *32*, 309–319.

(20) Hochstrasser, R. M. *The Journal of Chemical Physics* **1964**, *40*, 2559–2564.

(21) Adhikari, S.; Spaeth, P.; Kar, A.; Baaske, M. D.; Khatua, S.; Orrit, M. *ACS Nano* **2020**, *14*, 16414–16445.